Towards a dual phase grating interferometer on clinical hardware

Johannes Bopp[a], Veronika Ludwig[b], Michael Gallersdörfer[b], Maria Seifert[b], Georg Pelzer[b], Andreas Maier[a], Gisela Anton[b], and Christian Riess[a]

[a]Pattern Recognition Lab, Friedrich-Alexander-University Erlangen-Nuremberg, Martensstr. 3, 91058 Erlangen, Germany
[b]Erlangen Centre for Astroparticle Physics, Friedrich-Alexander-University Erlangen-Nuremberg, Erwin-Rommel-Str. 1, 91058 Erlangen, Germany

ABSTRACT

In the last decades, several interferometric phase sensitive X-ray imaging setups with highly incoherent sources were developed. One of the clinically most promising setups is the Talbot-Lau interferometer. However, these systems still suffer from some challenges that prevent their clinical use. One challenge is the post-patient attenuation of the analyzer grating, that doubles the effective dose. To address this issue, new setup designs were proposed using a second phase grating, instead of the absorbing analyzer grating. Those two phase gratings together can create a beat pattern at the detector that can be resolved by the detector directly. In this paper the simulation tool CXI is validated for dual phase grating setups. Using the simulation, we found an optimal setup using existing gratings. A first feasibility study is shown with two phase gratings of 4.12 and 4.37 µm. The computed visibility of 4.6 % in simulation is in good accordance with the experimental visibility of 4 %. The final visibility is a trade-off between the inter-grating distance, grating-detector distance, the beat period and the point spread function of the detector.

Keywords: Phase contrast imaging, Talbot-Lau, Grating based interferometry, Dual phase grating

1. INTRODUCTION

X-ray phase contrast imaging (PCI) can provide improved soft-tissue contrast for medical imaging tasks. There are multiple phase sensitive setups that can provide additional information besides classical attenuation images. The Talbot-Lau interferometer (TLI) is a promising setup for clinical use. It has only low requirements on the coherence of the source.[1] The TLI can therefore be operated with a standard clinical X-ray source. Besides a normal detector, three gratings have to be placed within the beam line (Fig. 1a). The source grating G_0 in front of the detector splits the beam into multiple different slit sources, thereby creating a partially coherent wave front. The phase grating G_1 imprints a phase modulation onto the wave. Due to the Talbot-effect, the grating pattern reappears at the Talbot-distances as self images in the intensity values.[2] Phase shifts by objects in the beam line cause a shift of the intensity pattern at the detector. To be able to resolve the pattern and the shifts, the analyzer grating G_2 is required. It has the same period as the self images, and by moving it in equidistant fractions of its period, a phase stepping curve is sampled. For reconstruction of the three signals, attenuation, differential phase and the so-called dark-field, a sine curve is fitted to the measurements for each pixel. By comparing the fit of an object scan with the fit of a reference scan without an object, the three images can be reconstructed (Fig. 2). The sine fit of the reference scan ($\mathbf{r}$) provides one quality measure, the so-called visibility v which can be calculated by

$$v = \frac{\max(\mathbf{r}) - \min(\mathbf{r})}{\max(\mathbf{r}) + \min(\mathbf{r})} \quad . \tag{1}$$

Further author information: (Send correspondence to J.B.)
J.B.: E-mail: Johannes.Bopp@fau.de, Telephone: +49 9131 85 27894, http://www5.cs.fau.de/~bopp

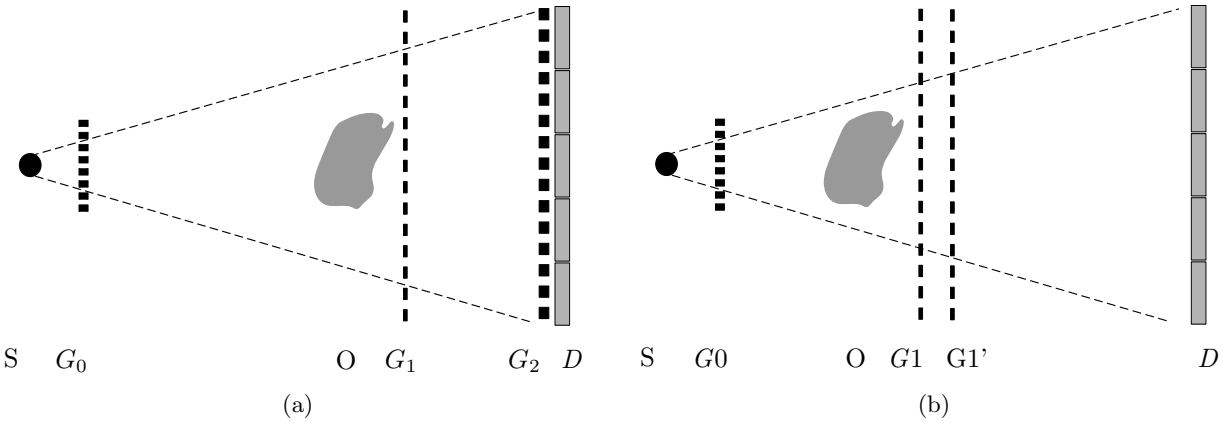

(a) (b)

Figure 1: The two setups discussed in this paper. In (a) the traditional TLI, with the source S, the optional G_0 grating, the phase shifting G_1 grating, and the absorbing analyzer grating G_2 in front of the detector D. In (b) the adapted TLI with a second phase grating G_1' instead of the G_2 grating. In both cases the object of interest O will typically be placed right in front G_1.

An alternative way of calculating the visibility is by the Fourier transform (indicated by the hat) of the fitted sine function

$$v = 2\frac{\hat{\mathbf{r}}[1]}{\hat{\mathbf{r}}[0]} \quad . \tag{2}$$

Some challenges need to be adressed before the TLI can be used in the clinical routine. One of them is caused by the analyzer grating. It introduces a post patient attenuation of about 50 %. Since ionizing radiation is harmful for the patient, it is desireable to find a setup design that allows to omit G_2. In standard TLI setups, G_2 is required because the self images created by G_1 grating are in the range of a few micrometers, and cannot be resolved by medical detectors directly. Miao *et al.* and Kagias *et al.* showed that it is possible to perform

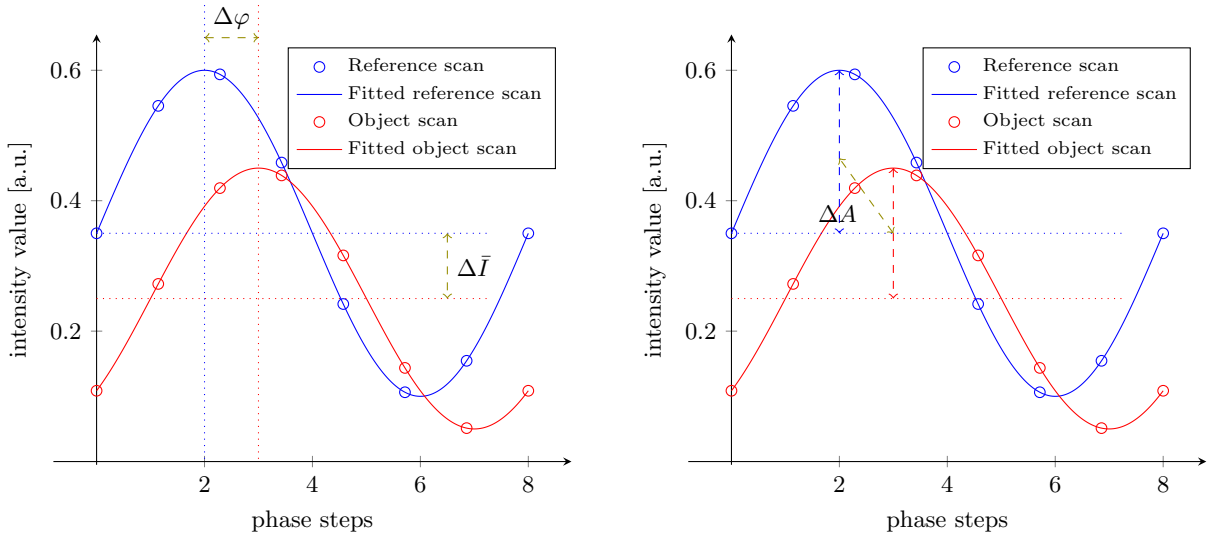

Figure 2: In the left plot the 8 phase steps of an ideal noise free reference scan with blue circles and the ideal object scan with red circles. The solid lines are the fitted sin curves. The phase shift for this particular pixel can be extracted by calculating $\Delta\varphi$. The attenuation value can be reconstructed by $\Delta\bar{I}$. The dark-field is computed as the ratio between the reference visibility and the object visibility as in Eqn. 1.

X-ray PCI by replacing the G_2 grating with a second phase grating G_1' (Fig. 1b).[3,4] However, these experiments were both performed with rather small grating periods.

In this paper, we take several steps towards translating the idea of two phase gratings to more realistic clinical parameters. Specifically, we report experimental measurements and simulations on grating periods that can be reliably produced, and on a detector with a point spread function (PSF) that is comparable to a clinical system. We particularly investigate the impact of grating positions for dual phase grating setups to validate our simulation tool CXI.[5]

2. METHODS

In a first step the numerical simulation tool CXI simulated an setup for existing gratings to be validated with experimental data. In this experiment, we seek a setup with two Nickel phase gratings, both with a height of 8.7 µm, and periods of 4.12 µm and of 4.37 µm, respectively. The setup further consists of a micro focus tube with a focal spot size of 9.5 µm and a detector with a pixel pitch of 50 µm. The length of the whole setup is constrained to 1.5 m. The simulation is constrained to create a beat pattern at the detector with a period of 300 µm, and the distance between focal spot and G_1' is constrained to arrange of 50 and 135 cm. For the simulation a typical transmission x-ray spectrum was used with a 40 kVp peak voltage.

To create a beat pattern the effects of the two phase gratings onto the wave can be approximated as adding two cosine functions. The wave can be approximated by

$$\Phi\left[\cos\left(\frac{2\pi x}{p_1^{\mathrm{proj}}}\right)+\cos\left(\frac{2\pi x}{p_1'}\right)\right] \quad , \tag{3}$$

where p_1^{proj} is the projected period of the first grating onto the G_1' plane, and p_1' the period of the grating G_1'. Adding two cosine functions results in a beat pattern with a period p_b of the envelope function of the difference of the frequencies of the two periods

$$p_b = \frac{1}{\mathrm{abs}\left(\frac{1}{p_1^{\mathrm{proj}}}-\frac{1}{p_1'}\right)} \tag{4}$$

at the G_1' plane. Important here is, due to the ambiguity of the abs-function, there are two possible p_1^{proj} resulting in the same p_b. The two p_1^{proj} can be translated in two different inter grating distances. Depending on the absolute position in the beam line and the resulting beat period the inter grating distance can vary. Therefore, in the following it will be named small and large. The beat pattern afterwards gets magnified at the detector

$$p_b^{\mathrm{det}} = \frac{p_b}{\mathrm{dist}(S-G_1')}\cdot\mathrm{dist}(S-D) \tag{5}$$

where $\mathrm{dist}(S-G_1')$ is the distance between the source and the grating G_1' and $\mathrm{dist}(S-D)$ is the distance between the source and the detector resulting in p_b^{det}. Since p_b is calculated with the absolute value of a difference, there are two possible positions for a grating with a fixed period to create the same beat period. Therefore, the grating G_1' can be placed on different positions on the Talbot carpet created by G_1.

Using Eqn. 5 the necessary beat period at the G_1' plane can be calculated to get a projected period at the detector of 300 µm. This allows to calculate the distance between the two gratings for a fixed projected period. Thus, only the positioning of the gratings in the beam line needs to be optimized in the simulation. The best setup will be validated experimentally.

In the next step the previously fixed beat period created in the detector plane was varied in in a range between 200 and 1000 µm in the simulation. A trade-off between the reduced visibility due to the PSF versus a reduced visibility due to the higher beat period at the detector was investigated.

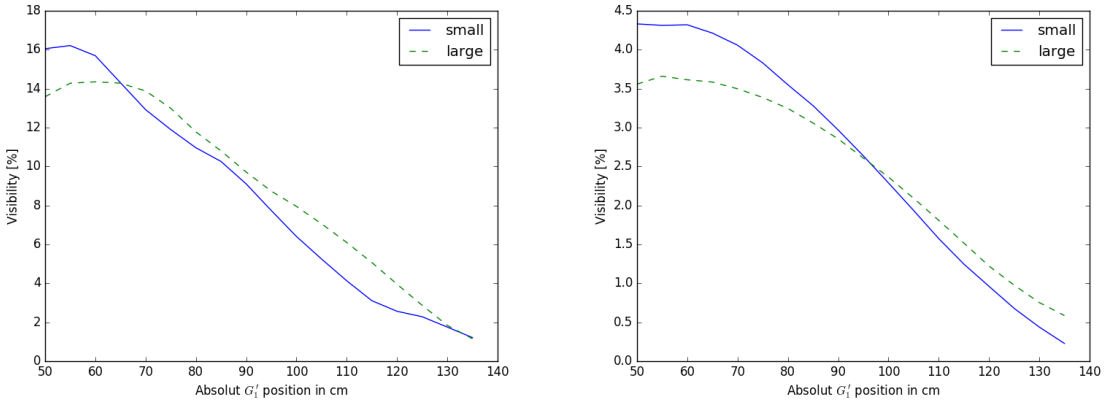

(a) (b)

Figure 3: Visibility versus different source-G_1' distances. In (a) the visibility calculated by the initial simulation is shown. In (b) the visibility after convolution of the simulated detector signal with the measured PSF of the detector is shown. In both plots the blue line is the smaller distance between the two gratings, the green dashed line the larger possible distance due to the ambiguity of the absolute value function.

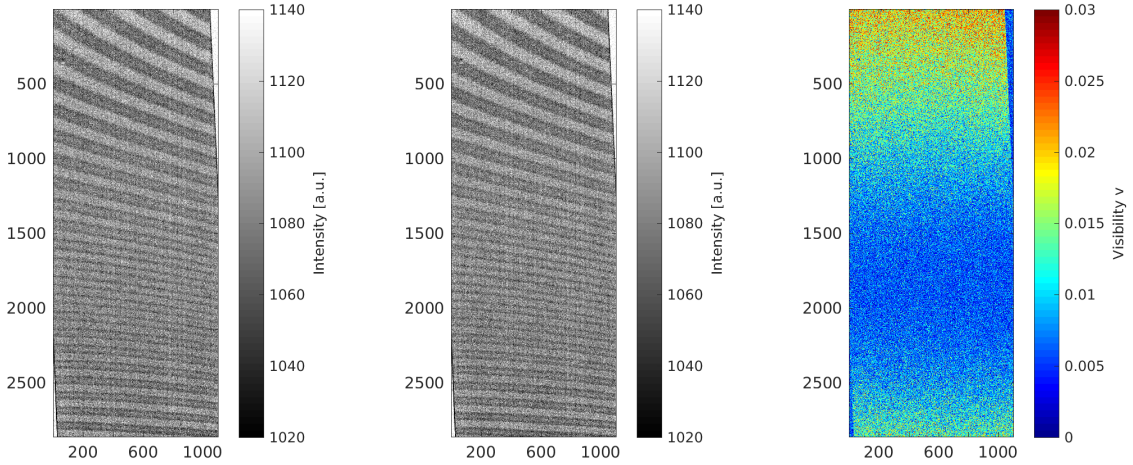

(a) (b) (c)

Figure 4: In (a) and (b) show two complimentary phase steps. (c) shows a visibility map over the whole grating area, computed from a least-squares sine fit. These visibilities are somewhat lower than 4 % due to noise artifacts in the least squares fit.

3. RESULTS

The results for the simulation showed an optimal visibility of 16 % at a position of the G_1' grating at 0.5 m downstream of the source. The necessary distance between the gratings was 3.8 cm. For G_1 the grating with a period of 4.12 µm was used, and the G_1' was the 4.37 µm grating. The simulated visibility for the different distances of the grating G_1' to the detector are shown in the plots in Fig. 3. The left plot shows the initial results without taking the PSF of the detector into account, while the right plot does. The blue and green lines show the results for the smaller and larger G_1-G_1' distances, respectively due to the distance ambiguity in Eqn. 4. The visibility difference can be explained by the different positions of the G_1' on the Talbot-carpet caused by G_1. Generally, larger G_1'-detector distances lead to higher visibility.

This system was experimentally set up. The fringe visibility for a line plot was around 4 %. The results of our experimental setup can be seen in Fig. 4.

The results of compromise between beat period at the detector and the detector PSF can be seen in Fig. 5.

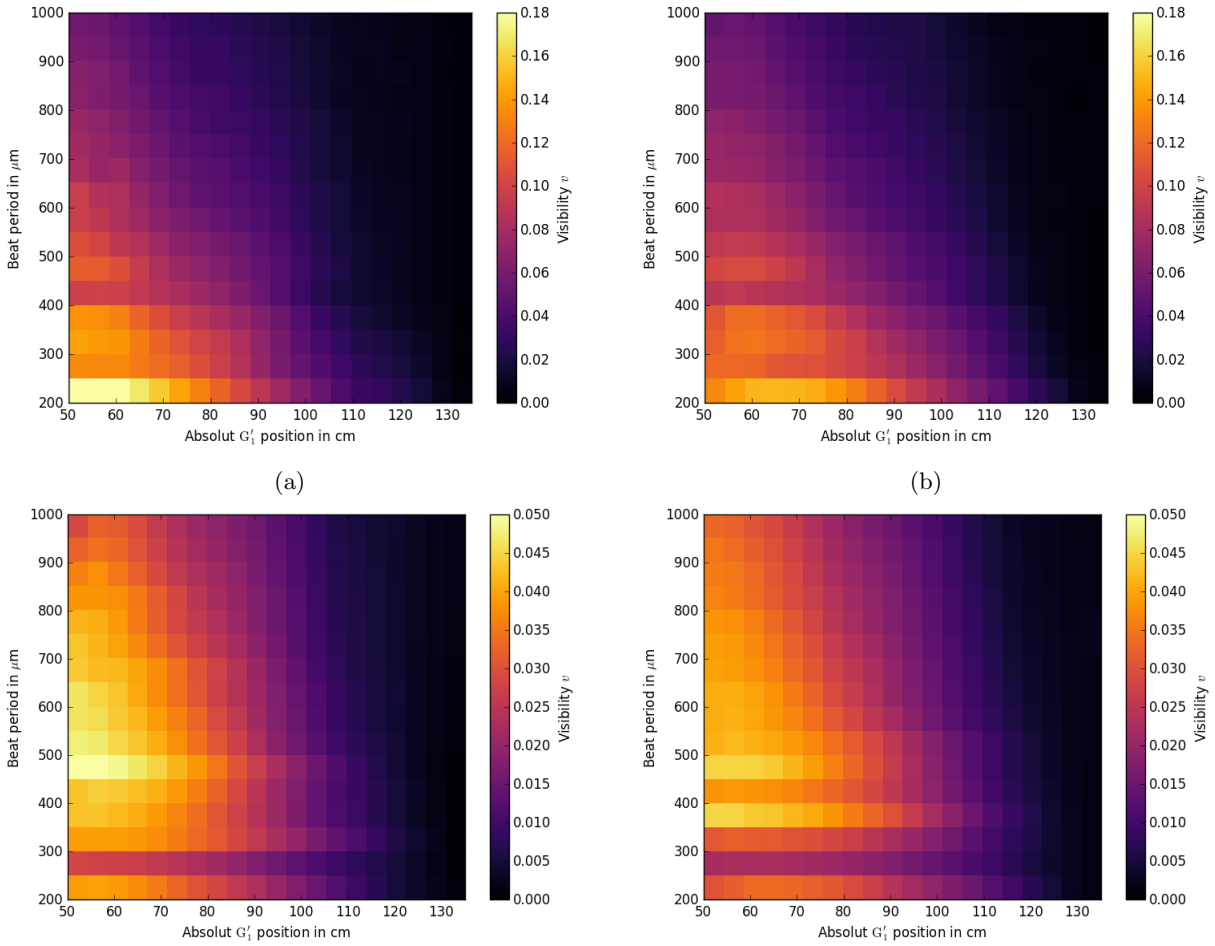

Figure 5: Results of the simulation for different beat periods on the y-axis and different positions of the position of the G_1' grating behind the focal spot on the x-axis. The simulated visibility is color coded in the same range for each row. In the top row are the results without the PSF, while in the bottom row are the results including the PSF into the simulation. On the left hand-side is the smaller inter-grating distance. The right hand-side shows the larger inter-grating distance. It can be seen that with the PSF included, the best visibility can be reached at 450 µm beat period for the smaller grating distance, and a visibility of around 5 %.

On the x-axis the absolute distance of the G_1' grating from the source is varied, the y-axis shows the beat period at the detector between 200 and 1000 µm. Figure 4 is a line plot created with the beat period of 300 µm. The possible visibility is color coded, and for each row, indicating the smaller inter-grating distance on the left, and the larger inter grating distance on the right, the same.

4. DISCUSSION AND OUTLOOK

The results show that there is an interaction between visibility, distance between G_1' and the detector, as well as the period of the fringes at the detector. After taking into account the point spread function (PSF) (Fig 3b) of the specific detector, the simulated results are in good accordance to the experiments. The simulations showed a visibility of 4.4 %, while the experimental results for a single shot were 4 %. The remaining difference can be explained by noise, the imperfect gratings, and the uncertainty regarding the exact spectrum of the X-ray source. At the bottom of Fig. 5 (c) and (d), at a beat pattern of 250 µm, there is one line with a noticeably reduced visibility. This is due to the particular shape of the wave front reaching the detector. The maxima are

very broad with only small minima, which are canceled out by the PSF resulting in a reduced or almost vanished visibility.

The highest visibility can be seen in the boundary area, in which the period of the pattern is larger due to magnification. This indicates that the fixed beat period at the detector can be optimized regarding the visibility with respect to the PSF. With the variation of the beat pattern at the detector a few percentage of visibility could be gained. The main points to increase the visibility would be to use gratings specially designed for a dual phase grating setup like Miao *et al.* and Kagias *et al.*[3,4] did. It would be possible to create smaller periods, the limiting factor here was the G_2 grating with the need of a high aspect ratio. The grating periods could be optimized for a certain spectrum, with periods to have an optimal inter-grating distance and to create an optimal beat pattern at the detector. For the grating design it would be interesting to investigate the impact of the duty-cycle of the phase gratings like shown by Rieger *et. al.*[6] For the given setup the visibility could be optimized by increasing the propagation distance behind G_1'.

In the next steps gratings and grating parameters should be simulated to increase the visibility. The gratings used for these experiment and the simulation can be far from ideal for the dual phase grating measurements. With the validated simulation it is possible to investigate different parameters and larger parameter spaces for better results.

ACKNOWLEDGMENTS

The work has not been published or sent to publication elsewhere. The authors gratefully acknowledge funding by Siemens Healthineers.

REFERENCES

[1] Pfeiffer, F., Weitkamp, T., Bunk, O., and David, C., "Phase retrieval and differential phase-contrast imaging with low-brilliance x-ray sources," *Nature physics* **2**(4), 258–261 (2006).

[2] Talbot, H. F., "Lxxvi. facts relating to optical science. no. iv," *The London and Edinburgh philosophical magazine and journal of science* **9**(56), 401–407 (1836).

[3] Miao, H., Panna, A., Gomella, A. A., Bennett, E. E., Znati, S., Chen, L., and Wen, H., "A universal moiré effect and application in X-ray phase-contrast imaging," *Nature Physics* **12**, 830–834 (2016).

[4] Kagias, M., Wang, Z., Jefimovs, K., and Stampanoni, M., "Dual phase grating interferometer for tunable dark-field sensitivity," *Applied Physics Letters* **110**(1), 014105 (2017).

[5] Ritter, A., Bartl, P., Bayer, F., Gödel, K. C., Haas, W., Michel, T., Pelzer, G., Rieger, J., Weber, T., Zang, A., et al., "Simulation framework for coherent and incoherent x-ray imaging and its application in talbot-lau dark-field imaging," *Optics express* **22**(19), 23276–23289 (2014).

[6] Rieger, J., Meyer, P., Pelzer, G., Weber, T., Michel, T., Mohr, J., and Anton, G., "Designing the phase grating for talbot-lau phase-contrast imaging systems: a simulation and experiment study," *Optics Express* **24**(12), 13357–13364 (2016).